# Laser heating and evaporation of a single droplet

S. Pokharel,[1] A. Tropina,[1] and M.N. Shneider[2]
[1)]*Department of Aerospace Engineering, Texas A&M University, TX 77843*
[2)]*Department of Mechanical and Aerospace Engineering, Princeton University, NJ 08544*

(*Electronic mail: pokharel_sagar@tamu.edu)

(Dated: 10 October 2022)

The laser technology is being abundantly studied for controlled energy deposition for a range of applications in aerodynamic flow control, material processing, ignition, and combustion. The absorption of laser radiation by liquid droplets affects further propagation of laser in the atmosphere and causes bleaching of suspended droplets while the ignition and combustion characteristics in combustors are influenced by the evaporation rate of the sprayed fuel. In this work, we present a multi-dimensional mathematical model built on OpenFOAM for laser heating and evaporation of a single droplet in the diffusion dominated regime taking into account absorption of the laser radiation, evaporation process and vapor flow dynamics. The developed solver is validated against available experimental and numerical data for the ethanol and water droplet heating and evaporation. For continuous heating the peak temperature is established by the balance of cooling, evaporation and heating and results in high temperature for larger droplets. It has been shown that for heating by a single laser pulse the maximum temperature of droplets depends only on the peak intensity of the laser radiation. Furthermore, for the peak irradiance close to the transition to the boiling regime, temporal dynamics of the droplet temperature is independent of the droplet size. With proper normalization of time, the dynamics of the droplet shrinkage and cooling is shown to be independent of droplet sizes and peak laser intensities. The influence of cooling and evaporation processes on droplet heating was found to be controlled by the pulse repetition rate for repeated pulse operation.

## I. INTRODUCTION

The evaporation of liquid droplets has been studied for a long time because of its applications in various multidisciplinary fields. Most popular applications include liquid fuel spray evaporation and combustion in high-pressure conditions, spray drying and cooling, material processing, crystal growth, medical aerosols, etc. Heating and evaporation of a liquid fuel droplet is the first important step in the ignition process. In addition, in the environmental sciences the theory of raindrops falling, fog and cloud formation at high altitudes can be significantly improved by knowledge of the processes associated with the evaporation of liquid droplets[1]. Thus a fundamental understanding of the droplet evaporation process and possible control of this process are of great importance for industrial engineering, bio-medical fields, and environmental sciences. Despite the continued research efforts in experiments and modeling of the droplet heating and evaporation, the physics of processes on the fluid-gas interface especially for arbitrary shape droplets is still not well-understood[2]. One of the difficulties in mathematical modeling is connected with the fact that the phase change process at the liquid-gas interface can be in non-equilibrium thus requiring molecular dynamics or the kinetic modeling approach.

In general, the fuel droplet evaporation process includes two sub-processes; detachment of fuel molecules from the drop surface (phase change), and diffusion of the formed vapor from the surface to the ambient gas. Assuming that the fuel vapor is saturated, the evaporation process is controlled by the vapor diffusion into the gas and can be described by hydrodynamic models of evaporation[3] started from the classical Maxwell diffusion theory. Diffusion hydrodynamic models describe well the evaporation of large droplets, but for small droplets, the evaporation process is limited by detachments and the release of fuel molecules from the droplet surface. In that case, we have so-called depletion or kinetic regime of evaporation, thus kinetic or molecular dynamics models are needed. A comprehensive description of results and unsolved problems in modeling heating and evaporation of spherical and non-spherical fuel droplets is presented in review papers[2,4]. The analytical solution to the heat and mass transfer problem for axis-symmetric spheroidal droplets is shown in[5]. Other models, which include the non-uniformity of the droplet temperature, effects of the internal circulation inside the droplet, and Stefan-flow are formulated in the papers of Abramzon and Sirignano[6]. Those models are extensively used as evaporation models in CFD calculations.

When laser radiation is used to heat a liquid droplet with a possibility of plasma formation near the droplet, new physical effects can be observed. In this case, droplet heating takes place via absorption of the laser radiation penetrating the droplet's surface, followed by the evaporation process. An optically transparent large fuel droplet behaves as an optical focusing system thus increasing the intensity of the incident laser radiation inside the droplet. Another effect is connected with the negative charge accumulation on the droplet due to the attachment of electrons from the surrounding plasma thereby introducing a strong electrostatic force on the droplet. Surface reactions and penetration of excited species through the liquid droplet interface can also take place[7]. It was shown in[8], that applying an external voltage across the droplet causes an appearance of the ionic wind, which in turn, enhances a heat transfer on the droplet interface. Possible control of the heating and evaporation processes using laser energy deposition is also attractive for modern aerospace applications, e.g, efficient mixing, ignition and combustion of liquid fuel droplets, laser wave propagation/attenuation in remote sensing, bleaching and control of size distribution of droplets, etc,

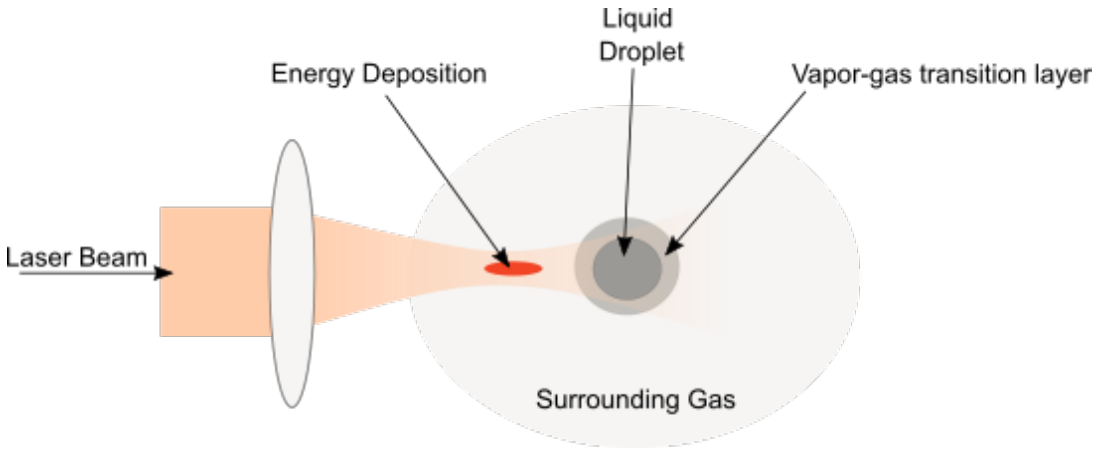


FIG. 1. Schematic of laser heating of droplet (not to scale).

thus understanding of effects connected with the laser irradiation of liquid fuel droplets is highly desirable. In this paper, we consider the first step towards the research related to the controllable heating and evaporation of the ethanol ($C_2H_5OH$) droplet using the continuous and pulsed laser energy addition which can be extended to study the non-equilibrium laser plasma formation and its interaction with the fuel droplet as shown in Fig. 1. Because of ethanol's advantageous properties such as renewable and biodegradable fuel and high latent heat, it is regarded as an alternative to conventional fuels[9]. Evaporation due to heating from ambient surrounding for ethanol and ethanol/diesel blends have been the focus of various recent studies[10,11]. Study of laser heating and evaporation of ethanol droplets and its control would be beneficial for laser communications and remote sensing, spray combustion and ignition, etc. Furthermore, the ionization potential of ethanol is lower compared with the air molecules which gives additional possibilities for fuel reforming and coupling with the laser-induced plasma.

The laser radiation absorption by a spherical droplet can be characterized by the Mie size parameter $\alpha = \frac{2\pi R}{\lambda} n$, where $R$ is the droplet radius and $\lambda$ is the laser wavelength and $n$ is the refractive index of the gas medium. For small $\alpha$ the internal distribution of the electric field, as well as the temperature distribution within the droplet, can be considered uniform. For droplets with $\alpha > 1$, as the thermal conductivity of liquid ethanol is high compared to the gas phase the laser radiation absorption can be assumed uniform if the intensity is not high enough to transition to explosive evaporation. To describe the uniform laser radiation absorption in spherical droplets an approach similar to[12,13] can be used where authors derived simple approximate expressions for the absorption efficiency factor on the basis of the Mie theory[14] for arbitrary size of droplets. Similar approaches can be found in other literature sources[15–17]. The liquid droplet interacts with the surrounding gas through mass, momentum, and energy exchanges. A hydrodynamic model based on the thermodynamic equilibrium at the droplet interface, attributed to Maxwell, suggests that the vapor concentration in the vicinity of the droplet surface is saturated and the rate of evaporation is controlled by the vapor diffusion to the ambient gas. Following the hydrodynamic model, the commonly known $D^2$-law provides a relationship between the droplet diameter and the vaporization time, assuming the uniform temperature and steady evaporation. The reliability of the hydrodynamic models could be increased by the use of jump conditions across the Knudsen layer (the thin region between the liquid droplet interface and hydrodynamic region). Most empirical correlations for the droplet heating and evaporation are integrated through the gas phase with thermophysical properties taken at the reference gas state and include empirical correlations, as functions of Nusselt, $Nu$ and Sherwood, $Sh$ numbers, based on previous analytical, computational and experimental studies. Since the evaporation process of an isolated droplet at small $\alpha$ is spherically symmetrical there is no need for multi-dimensional models. The laser heating and evaporation of isolated droplet, below the breakdown threshold for the ambient gas, is also spherically symmetric provided that the waist size of the laser is big compared to the size of the droplet, $\omega_0 > R_d$. But an immediate extension to simulate multiple droplets ( array of droplets ) or interaction with in-homogeneous ambient surrounding ( laser induced plasma ) requires a multidimensional model. Thus a general two-dimensional axisymmetric model of droplet heating and evaporation was developed using the open-source library OpenFOAM. To develop a consistent model for the fuel droplet interaction with the laser pulse, Navier-Stokes and species concentration equations should be coupled with the diffusion dominated droplet evaporation model. In this paper, we present a two-dimensional mathematical model of the laser heating and evaporation of the ethanol droplet, which can be extended to include the laser plasma formation and interaction.

## II. FORMULATION OF THE MODEL

### A. Liquid Droplet

Although the size of the droplet decreases due to the evaporation process it is considered to be spherical and uniformly

heated so the equation for the total enthalpy of the droplet is sufficient to describe the heating and evaporation process in the droplet. Integration of the energy equation over the spherically symmetrical droplet volume gives Eq.1 which describes the evolution of temperature of the droplet in time. Because the thermal conductivity of the liquid is higher compared to the gas phase the uniformity in the temperature distribution inside the droplet is assumed to be achieved instantaneously relative to equivalent energy equilibration in gas phase ( $\approx$ 1 ms compared to 10 ms ) . Only for the case of relatively high laser intensity, corresponding to the explosive regime of evaporation, a non-uniform distribution of temperature inside the droplet is important. Here we are presenting results for the so-called slow heating regime and therefore an integrated approach for heating and absorption is considered. Since we are not solving the equation for the temperature distribution inside the droplet, the heat flux at the surface $-K_D \frac{\partial T_L}{\partial r}\Big|_R$ must be replaced by a consistent energy balance[18] at the interface which results in Eq.2.

Here, $C_{p,D/g}$ is the specific heat capacity at constant pressure for the droplet($D$) or gas ($g$). $T_D$ is the integrated temperature inside the droplet, $T_{D0}$ is the initial droplet temperature while $T_g$ is the temperature of the bulk gas. $\rho_{D/g/v}$ is the mass density for a drop, gas, or vapor. Similarly, $K$ is the thermal conductivity, $U$ is the bulk velocity normal to the interface and $R$ is the droplet radius. The mass and energy flux are $m_f$ and $w_f$, respectively. Mass flux, $w_f$, is calculated using Eq.3 which results from energy balance at the liquid droplet interface. $Q_v$ is the rate of the heat absorption by the liquid droplet due to laser radiation and $L$ is the latent heat of vaporization.

$$C_{p,D}\frac{d(4/3\pi R^3\rho_D T_D)}{dt} = 4\pi R^2 K_D \frac{\partial T_L}{\partial r}\Big|_R + Q_v \qquad (1)$$

$$4/3\pi R^3\rho_D C_{p,D}\frac{dT_D}{dt} = -4\pi R^2 m_f (L + C_{p,D}(T_g - T_D)) + 4\pi R^2 w_f + Q_v \qquad (2)$$

$$w_f = K_g \frac{\partial T_g}{\partial r}\Big|_R - \rho_g U C_{p,g} T_g\Big|_R - \frac{m_f^3}{2\rho_v^2} \qquad (3)$$

$$\frac{dR}{dt} = -\frac{m_f}{\rho_D} \qquad (4)$$

The energy flux through the interface, $w_f$, includes thermal conduction through the gas phase ( first term in the right-hand side of Eq.3), heat convection, and kinetic energy flux ( second and third terms in the right hand side of Eq.3, respectively). The latter results from the induced flow of the ethanol vapor. The term $m_f C_{p,D}(T_g - T_D)$ in Eq. 2 represents the enthalpy flux connected with the shrinkage of the droplet surface due to evaporation. Because of the droplet surface shrinkage an additional equation, Eq.4, for the temporal evolution of the droplet radius along with Eq.2 are solved. To close the system of equations 2 and 4, the initial radius and temperature of the droplet $R(t=0) = R_0$ and $T_D(t=0) = T_{D0}$ are provided. The boundary conditions at the interface are set through the specification of energy and mass fluxes $w_f$, $m_f$ which are taken from the hydrodynamic part of the model.

### B. Absorption of laser radiation

In this study we consider uniform heating from x-polarized light, the effects of absorption of laser radiation by the surrounding gas is neglected, gas ionization is also neglected because the intensity of the laser is considered to be well below the ionization threshold of the ambient gas. The uniform laser radiation absorption by the droplet is approximated as $Q_v = Q_a I_{L0} \pi R^2$, where $I_{L0}$ is the laser intensity. $Q_a$ is the efficiency factor of absorption, which according to the Mie theory[14] can be found using Eq.5. The deviation from uniform absorption increases with the drop size increase but for the sizes considered here, the assumption of the uniform absorption is valid. The semi-empirical expression,[12,17] utilized to approximate the efficiency factor of absorption from the Mie theory is $Q_a = \frac{4n}{(n+1)^2}(1 - exp(-8\,\pi k\, R\,/\,\lambda))$ , where $n$ and $k$ are the real and imaginary parts of the complex refractive index of the liquid droplet respectively and $\lambda$ is the laser wavelength. Comparison between the efficiency factor of absorption calculated by the approximate expression and using the Mie theory 5 is shown in Fig. 2 which justifies the use of the approximate equation for $Q_a$. Here $m = n - ik$ is the complex refractive index, $x$ is the Mie size parameter while the Mie coefficients, $a_k$ and $b_k$ are defined as follows; $\psi_k$ and $\zeta_k$ are the Riccati-Bessel functions.

$$Q_a = \frac{2}{x^2}\sum_{k=1}^{\infty}(2k+1)\left[Re(a_k) - |a_k|^2 + Re(b_k) - |b_k|^2\right] \qquad (5)$$

$$a_k = \frac{\psi_k(x)\psi_k'(mx) - m\psi_k'(x)\psi_k(mx)}{\zeta_k(x)\psi_k'(mx) - m\zeta_k'(x)\psi_k(mx)}$$

$$b_k = \frac{m\psi_k(x)\psi_k'(mx) - \psi_k'(x)\psi_k(mx)}{m\zeta_k(x)\psi_k'(mx) - \zeta_k'(x)\psi_k(mx),}$$

### C. Hydrodynamic part of the model

Equations for the temperature and species conservation and Navier-Stokes equations for the gas phase form the hydrodynamic portion of the mathematical model. This model provides the necessary boundary conditions for the energy and mass fluxes, which are required for coupling with the heating and evaporation model described in the previous section. The hydrodynamic model includes equations of conservation of the mass (Eq.6), momentum (Eq.8), and thermal energy

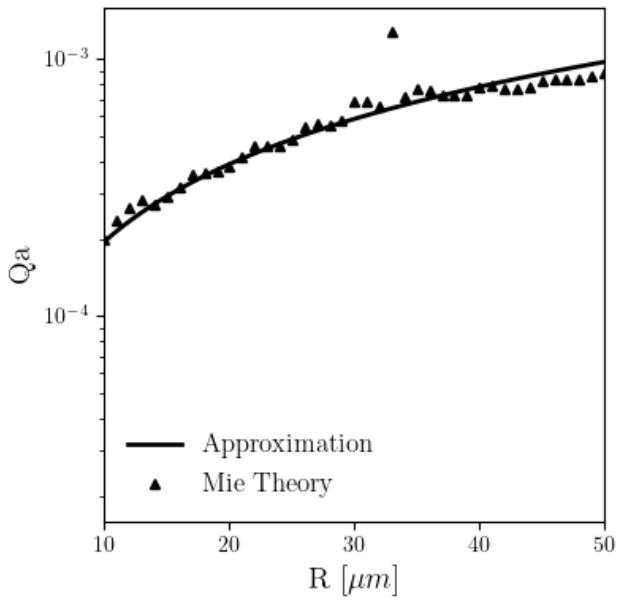


FIG. 2. Efficiency factor of absorption, $Q_a$ against radius of the droplet, $R$.

(Eq.9) of the fluid. Furthermore, equations for the conservation of individual species (Eq.7) are also included. Thus the system of equations (Eq.6-9) forms a complete model describing the behavior of a multi-component mixture in the gas phase.

$$\frac{\partial \rho}{\partial t} + \nabla \cdot (\rho \vec{v}) = 0, \tag{6}$$

$$\frac{\partial (\rho Y_k)}{\partial t} + \nabla \cdot (\vec{v} \rho Y_k) = \nabla \cdot (D \rho \nabla Y_k), \tag{7}$$

$$\frac{\partial (\rho \vec{v})}{\partial t} + \nabla \cdot (\rho \vec{v} \vec{v}) = -\nabla p + \nabla \cdot \vec{\vec{\tau}}, \tag{8}$$

$$\frac{\partial (\rho h)}{\partial t} + \nabla \cdot (\rho \vec{v} h) + \frac{\partial (\rho k)}{\partial t} + \nabla \cdot (\rho \vec{v} k) = \frac{dp}{dt} + \nabla \cdot \left( \vec{\vec{\tau}} \cdot \vec{v} \right) + \nabla \cdot (K \nabla h), \tag{9}$$

where $\vec{\vec{\tau}}$ is,

$$\tau_{ij} = \mu \left( \frac{\partial v_i}{\partial x_j} + \frac{\partial v_j}{\partial x_i} - \frac{2}{3} \frac{\partial v_k}{\partial x_k} \delta_{ij} \right)$$

are components of the viscous stress tensor, and $h$ is the mass specific enthalpy and $k$ is the kinetic energy. In the system of equations (6-9) for $\rho$, $\vec{v}$ and $p$ are density, velocity and pressure, respectively. $Y_k$ is the mass fraction of species $k$ while $D$ and $K$ are the mixture thermal conduction coefficient and mixture averaged diffusion coefficient. To close the set of equations we use the equation of state

$$p = \rho R_u T \sum_k^{N_s} \left( \frac{Y_k}{M_{w,k}} \right)$$

where $R_u$ is the universal gas constant and $M_{w,k}$ is the molecular weight of species $k$.

The momentum exchange between the droplet and the gas phase is neglected. With the specification of the normal bulk velocity $U$, the concentration of the ethanol vapor $Y_v$, and droplet surface temperature $T_D$ at the droplet interface, the hydrodynamic part of the model is coupled with the heating and evaporation model. The vapor mass flux $m_f = \rho Y_v U - D\rho \nabla Y_v$ being substituted in Eq.3 gives the required total mass and energy flux for the evaporation model. After the energy and mass flux are specified equations of the evaporation model can be integrated in time to find the updated average temperature and radius of the droplet. With no momentum exchange, zero gradient in pressure was assumed at the interface. The Clausius-Clapeyron equation is used to determine the mass fraction of ethanol vapor at the interface using the updated pressure and droplet temperature $T_D$. Only a normal bulk velocity is assumed to exist at the droplet interface which is specified from the calculated mass flux as $U = m_f/\rho$. Because the mass flux of species except the fuel vapor is zero, the total mass flux at the interface is equal to the total vapor mass flux. The remaining boundary conditions for the species' concentration $Y_k$ must be specified at the interface. We assume, that the mass flux of species (other than vapor) normal to the interface is zero and use this condition to find $Y_k$ at the interface formulating a Robin-type boundary condition.

$$\vec{\Gamma}_k = U \rho Y_k - D \rho \nabla Y_k = 0$$

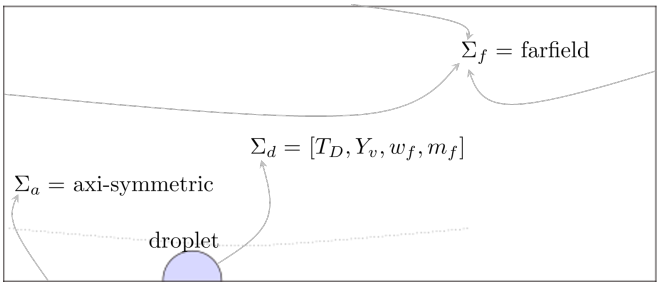


FIG. 3. Schematic diagram showing the boundary conditions for the coupled mathematical model.

The thermodynamic properties of ethanol liquid, vapor, and ambient gas depend on the temperature. We use a mass averaged approach for thermodynamic properties of the mixture, and the Wilkes mixing rule[19] for transport properties. The latent heat of vaporization and saturated vapor pressure are also functions of temperature taken from the NIST database. Other properties of ethanol in a liquid and vapor phase were collected from different sources,[20–23] and are provided in the Appendix.

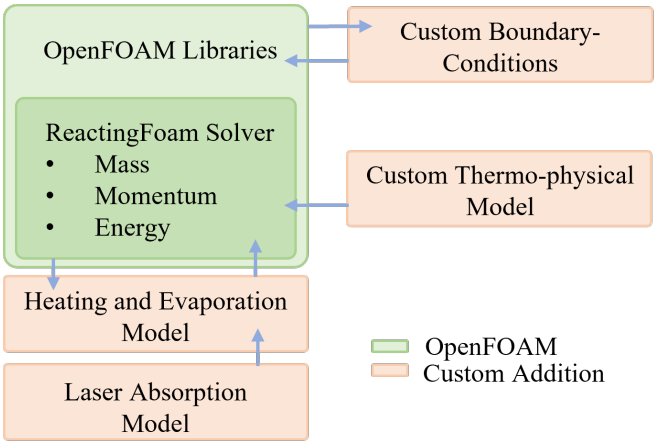


FIG. 4. Block scheme of the numerical solver built in OpenFOAM.

### D. Numerical procedure

To solve the system of equations (Eq.6-9) we developed a numerical solver using the finite-volume framework of libraries from OpenFOAM[24]. The open-source solver reactingFoam of OpenFOAM-v6 (OF) was extended to include the required thermophysical model for the vapor-air mixture. Similarly, we added the laser absorption model and the evaporation model combined with custom boundary conditions at the interface. Figure 4 shows the schematic diagram explaining the interplay between available OpenFoam libraries and added sub-sections specifically for the current work. As coupling between the velocity and pressure is important for the stability and for the accurate capturing of the induced Stefan-flow velocity we choose the PIMPLE algorithm with a bounded implicit Euler scheme for temporal integration. The convective and diffusion terms were discretized by the upwind-biased second order scheme and Gauss linear scheme with non-orthogonality correction, respectively.

### E. Verification and validation of the code

In the experimental study,[25] authors considered evaporation of the isolated ethanol droplet at atmospheric pressure for a number of ambient gas temperatures ranging from 373 K to 623 K. A special experimental setup was designed to minimize the conduction loss from the droplet to the fiber holding the droplet. We choose a case with the initial droplet diameter of $D_0 = 500\ \mu m$ at $T_D = 300\ K$ evaporating into the ambient air of temperature $T_g = 623\ K$ for the model validation. Figure 5 shows temporal dynamics of the normalized diameter of the droplet. It is seen that the surface area of the droplet decreases as evaporation progresses and the so-called $D^2$ regime is observed for steady evaporation caused by heating from the ambient surrounding gas. But as the droplet's size decreases the rate of evaporation slows and started to deviate from the $D^2$ law. The larger evaporation mass flux leads to higher losses in kinetic energy from evaporating vapor molecules and loss of enthalpy from the droplet shrinkage. Observed good agreement with the experimental results shown in Fig.5 indicate that the developed model can predict heating and evaporation of the droplet with high accuracy.

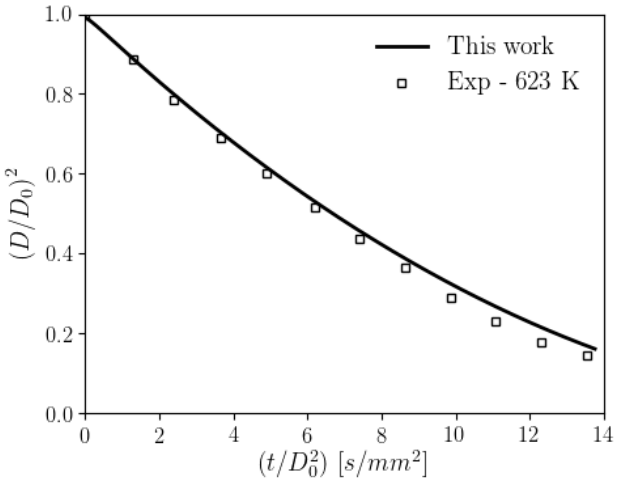


FIG. 5. Normalized diameter squared against normalized time, lines represent simulation results and symbols represent experimental results from[25].

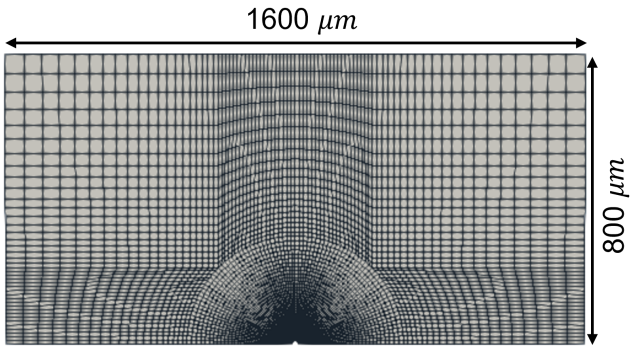


FIG. 6. Computational domain specifications used during verification.

Park and Armstrong[15] formulated a model for heating and evaporation of the water droplet continuously irradiated by a laser. For the diffusion dominated heating and evaporation they formulated a zero-dimensional model which solved for the droplet temperature $T_D$ and droplet radius, $R_d$ combined with the expressions for the mass and heat loss rate. We compare our results for the water droplet with the results from[15], where the water droplet of $R_0 = 10\ \mu m$ at 300 K was continuously irradiated by a $CO_2$ laser beam of the wavelength, $\lambda = 10.6\ \mu m$. Figure 7 shows the temporal evolution of the droplet temperature, $T_D$ for the different mesh sizes and compares the results with Park and Armstrong's[15]. The domain size for the case is shown in Fig.6. The fine mesh had 8750 cells with the smallest cell size being 0.3 $\mu m$, while the coarse one had 5600 cells with the smallest size 0.4 $\mu m$. Tempo-

ral dynamics of the droplet temperature is the same for fine and coarse meshes, thus our simulation results are mesh independent. As seen from Fig. 7 the maximum temperature of the irradiated droplet is in good agreement for both models. But we received a sharper increase in the droplet temperature compared to the Park and Armstrong's model[15]. We claim that the temporal dynamics is different mainly because of differences in the laser heating source formulation as the use of same optical parameters for the liquid droplet provided lower volumetric heating in the Park and Armstrong's model[15]. The model formulated in the paper[15] was zero-dimensional in the gas phase and was based on an approximate evaporation flux for steady formulation. This led to instant development of vapor concentration profile from the interface compared to unsteady development of the vapor concentration profile which is also captured in our formulation. Thus, the implementation details of the kinetic energy exchange and shrinkage of droplet are not comparable directly to our model. Furthermore, the droplet's temperature is susceptible to the thermophysical and optical properties of the liquid/vapor, which are constant in[15]. It also caused observed quantitative differences between the results. In fact, our model is able to capture the dynamics of laser heating and evaporation of the liquid droplet with adequate accuracy.

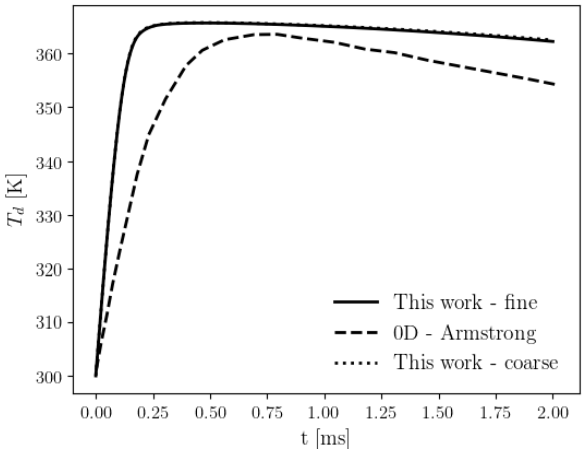


FIG. 7. Temporal evolution of the droplet temperature, solid line - results from this work for a fine grid (8750 cells), dotted lines - results for a coarse grid (5600 cells), and dashed line - results from the Armstrong's model[15];Water droplet of $R_0 = 10\ \mu m$ at 300 K, $\lambda = 10.6\ \mu m, I_0 = 10^7\ W/m^2$.

## III. RESULTS AND DISCUSSION

We consider continuous and pulsed laser heating and evaporation of the ethanol droplet at different laser intensities and droplet sizes and compare results with the available literature data. The results presented in the following sections are for laser with wavelength $\lambda = 1064\ nm$.

### 1. *Continuous laser heating*

Because studies on laser heating and evaporation of droplets had been performed mostly for water droplets, we also simulated laser irradiation of the water droplet. First, we compare the dynamics of continuous laser heating and evaporation of water and ethanol droplets of radius of 10 $\mu m$. The laser wavelength is taken as $\lambda = 1064\ nm$ with $I_{l0} = 10^{10}\ W/m^2$ and the initial droplet temperature $T = 300\ K$. Figure 8 shows a comparison between temporal dynamics of the droplet temperature and the normalized diameter squared for water and ethanol droplets. It is seen, that for the same laser intensity and size of the droplet the maximum temperature of the water droplet is higher by $\approx 12\ K$ than that of ethanol. Furthermore, because of the higher evaporation mass flow, the ethanol droplet shows a sharp decrease in the surface area. For example, at 2.5 $ms$ ethanol droplet has lost 70% of its surface area while the water droplet has lost only 40%. For both droplets, the temperature reaches a plateau after a sharp increase in evaporating fluxes. During early heating of the droplets, $t < 0.25\ ms$ when there is essentially no conduction and evaporation losses, temperature rise of the ethanol droplet is higher than for the water droplet. Although the absorption coefficient at $\lambda = 1064.0\ nm$ is larger for water compared to ethanol ( see appendix for refractive index values), higher $\rho C_p$ in water resists changes in the temperature. The peak temperature is determined by the balance of evaporation, laser absorption and conduction loss. Thus, heating and evaporation of the ethanol droplet with lower boiling temperature and higher evaporative losses results in a lower peak temperature.

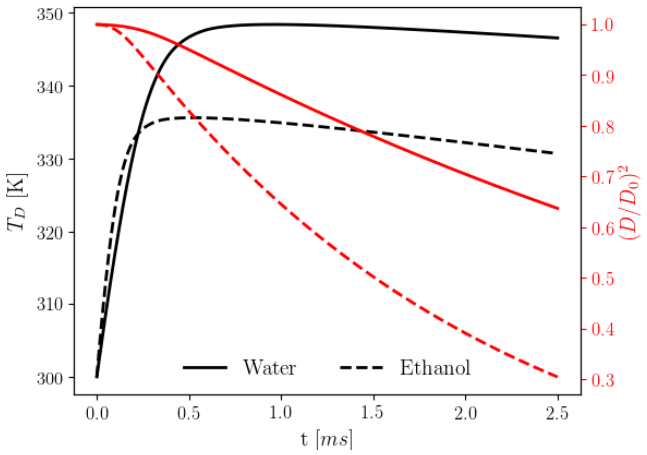


FIG. 8. Temporal evolution of the droplet temperature, left axis, and the normalized surface area, right axis for water (solid lines), and ethanol (dashed lines). $R_D = 10\ \mu m, I_{L0} = 10^{10}\ W/m^2$, the continuous laser heating source.

We also provide an analysis of heating and evaporation characteristics of ethanol droplets of different sizes $R_D = (10\ \mu m\ , 40\ \mu m)$. The same continuous laser heating source and ambient conditions as in Fig.8 were taken. Figure 9 shows results of the numerical simulation. It is seen that the initial

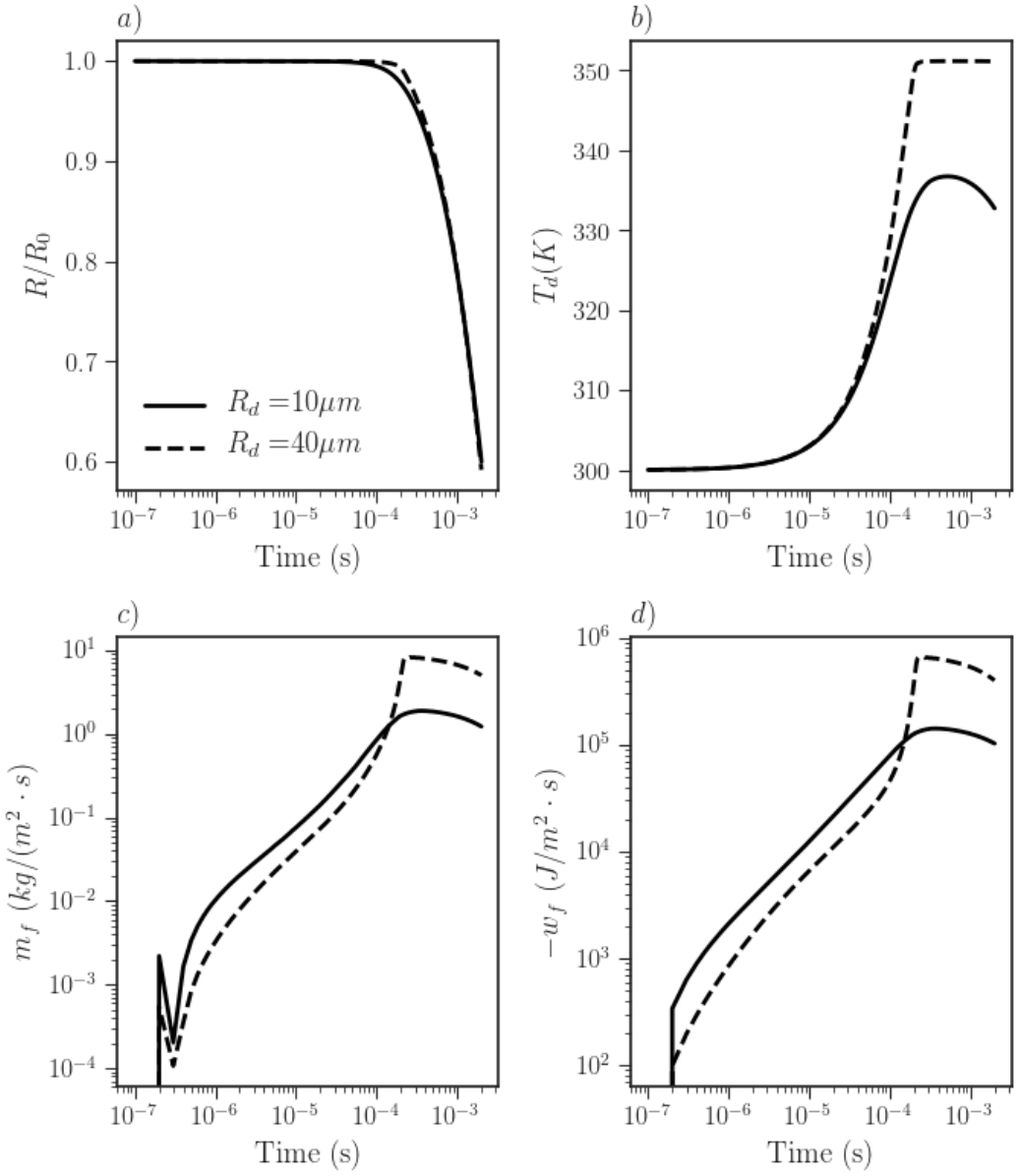


FIG. 9. Temporal evolution of ethanol droplet heating and evaporation during continuous heating; a) normalized radius, b) droplet temperature, c) evaporation mass flux, and d) conduction and convective heat flux. Solid lines represent droplet of size $R_D = 10\ \mu m$, and dashed lines represent droplet of size $R_D = 40\ \mu m$; $I_{L0} = 10^{10}\ W/m^2$ .

size of the droplet dictates the maximum droplet temperature. At the beginning of the simulation when the droplet is surrounded by the ambient gas, a small difference between the vapor concentration at the droplet interface and the surrounding gas results in a sudden diffusive flux. This flux equilibrates as soon as the vapor concentration establishes a continuous profile at the interface as shown in Fig.9,c. Since the initial mass flux is insignificant to the mass of the droplet, the spikes do not affect the results obtained. In the initial period of laser heating, both the mass flux Fig.9,c and heat flux Fig.9,d are small and negligible compared to the laser absorption. With progress in time these losses are higher for the smaller droplet which leads to a slower increase in the droplet temperature. Only when the maximum temperature is reached for both droplets the mass flux and heat flux from the larger droplet exceeds that of the smaller droplet. This tendency is also observed in temporal dynamics of the normalized droplet radius Fig.9. The higher temperature of large droplets irradiated by the laser of the same intensity is connected with the balance between energy loss per unit volume and the heat energy absorbed by the droplet per unit volume. The absorbed energy per unit volume for both droplets is not significantly different. The heat flux out of the droplet depends on the temperature gradient at the interface which is also comparable for

| $R_D$, $\mu m$ | 10 $\mu m$ | 25 $\mu m$ | 40 $\mu m$ |
|---|---|---|---|
| $I_{L0}$, $W/m^2$ | $0.5 \cdot 10^{14}$ | $1 \cdot 10^{14}$ | $5 \cdot 10^{14}$ |

TABLE I. Droplet radius and intensity range for the case of pulsed laser heating.

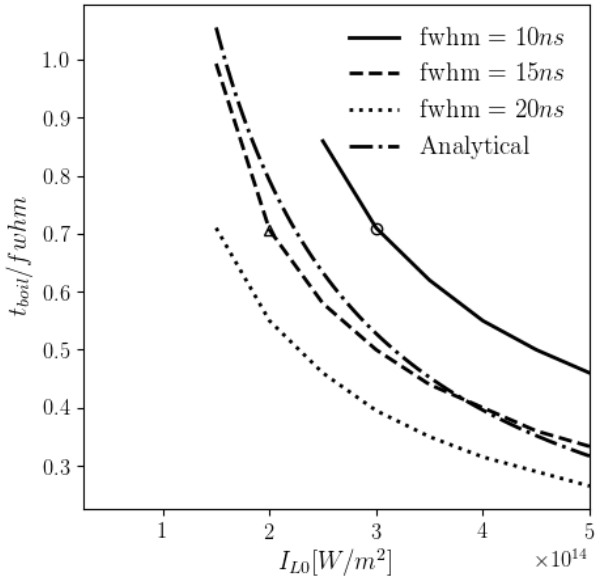


FIG. 10. Time required to reach boiling temperature normalized by fwhm against the peak laser intensity. Analytical results are normalized for $fwhm = 15$ $ns$. Symbols show results for two cases with same integrated intensity but different fwhm.

both droplets at the initial period of laser heating, because of the same initial droplet temperature. But the total heat energy loss per unit volume is smaller for the larger droplet because it scales as $q_v \propto 1/R_D$. Thus, relative cooling becomes stronger as the droplet size decreases due to which the temperature decrease is observed at later times for smaller droplets, while in larger droplets the heating is mainly balanced by evaporation and are maintained at relatively constant temperature. Considering continuous laser heating the laser intensity should be smaller than some critical intensity, which will guarantee that the droplet doesn't explode due to the very fast evaporation, or that the evaporation regime will not turn into boiling. One of the ways to avoid such transition is the use of the pulsed laser for heating and evaporation, which also provides additional possibilities for the evaporation process control.

### 2. *Pulsed laser heating*

Main parameters for the simulation in this section are shown in Table I. The laser wavelength is $\lambda = 1064$ $nm$ with full-width half maximum, $fwhm = 10$ $ns$, and droplets are evaporated into the ambient air at 300 $K$.

For pulsed laser heating of a droplet, due to the short duration of the single laser pulse, the evaporative processes have not yet been established. If the intensity of the laser pulse is high enough, the droplet will enter the boiling mode after absorbing enough laser radiation to reach the boiling temperature. In the cases, when the peak laser intensity was $I_{L0} = 5 \cdot 10^{14}$ $W/m^2$ for all droplet sizes considered, see table I, the droplet temperature exceeds the boiling temperature at $\approx 2$ $ns$ and the evaporating process goes into the boiling regime. As seen from previous results for continuous laser heating, shown in Fig.9,b, the initial rise of the droplet temperature caused by the laser irradiation is the same regardless of the droplet size. The same trend is observed for all droplets with pulsed laser heating when the high laser intensity resulted in a temperature above the boiling temperature.

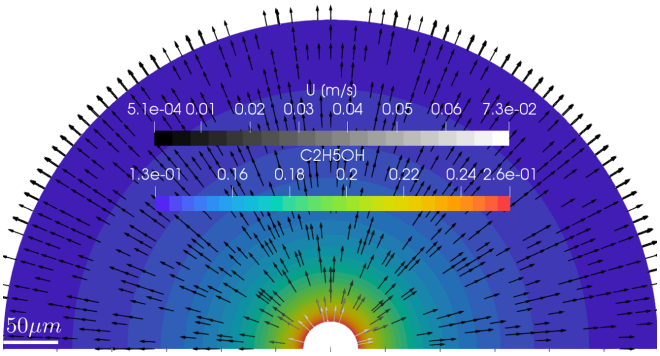


FIG. 11. Velocity vectors overlaid on the contours of mass fraction of ethanol at 1 $ms$ for pulsed laser heating. $fwhm = 10$ $ns$, $I_{L0} = 1.0 \cdot 10^{14}$ $W/m^2$ , $R_{D0} = 25$ $\mu m$ .

A detailed look into the time required for the droplets to reach the boiling temperature due to the absorption of the laser radiation can aid in the laser parameter selection for desired droplet heating and evaporation dynamics. The time required for ethanol droplets of sizes listed in table I to reach the boiling temperature was recorded by varying the laser intensity and pulse width. The time to reach the boiling temperature for the droplet normalized by the fwhm of the laser for a range of intensities is presented in Fig.10. The laser pulse had a Gaussian shape in time defined by the fwhm and peak intensity. As droplet heating was found to be independent of the droplet size (at early times for pulsed heating), results for the different sizes of droplets collapse into a single curve. Due to the higher absorption, an increase in the laser intensity causes a decrease in the time required to reach the boiling temperature and the dependence is non-linear. The time to reach the boiling temperature with a high intensity pulse is the time required for the droplet to increase its sensible enthalpy from the initial temperature to the boiling temperature as other heat losses are not significant on the considered timescale. Thus, at constant thermophysical properties of the liquid droplet and a constant laser intensity, the time to reach boiling is given by the relation, $t_{boil} = (4/3)R\rho_D C_{p,D}(T_b - T_a)/(Q_a I_L)$. It should be noted that $t_{boil}$ is independent of the radius of the droplet, $R$, because the approximation of efficiency factor of absorption, $Q_a$, is proportional to the droplet radius, $R$. Figure 10 also shows the analytical results for the case when the full-

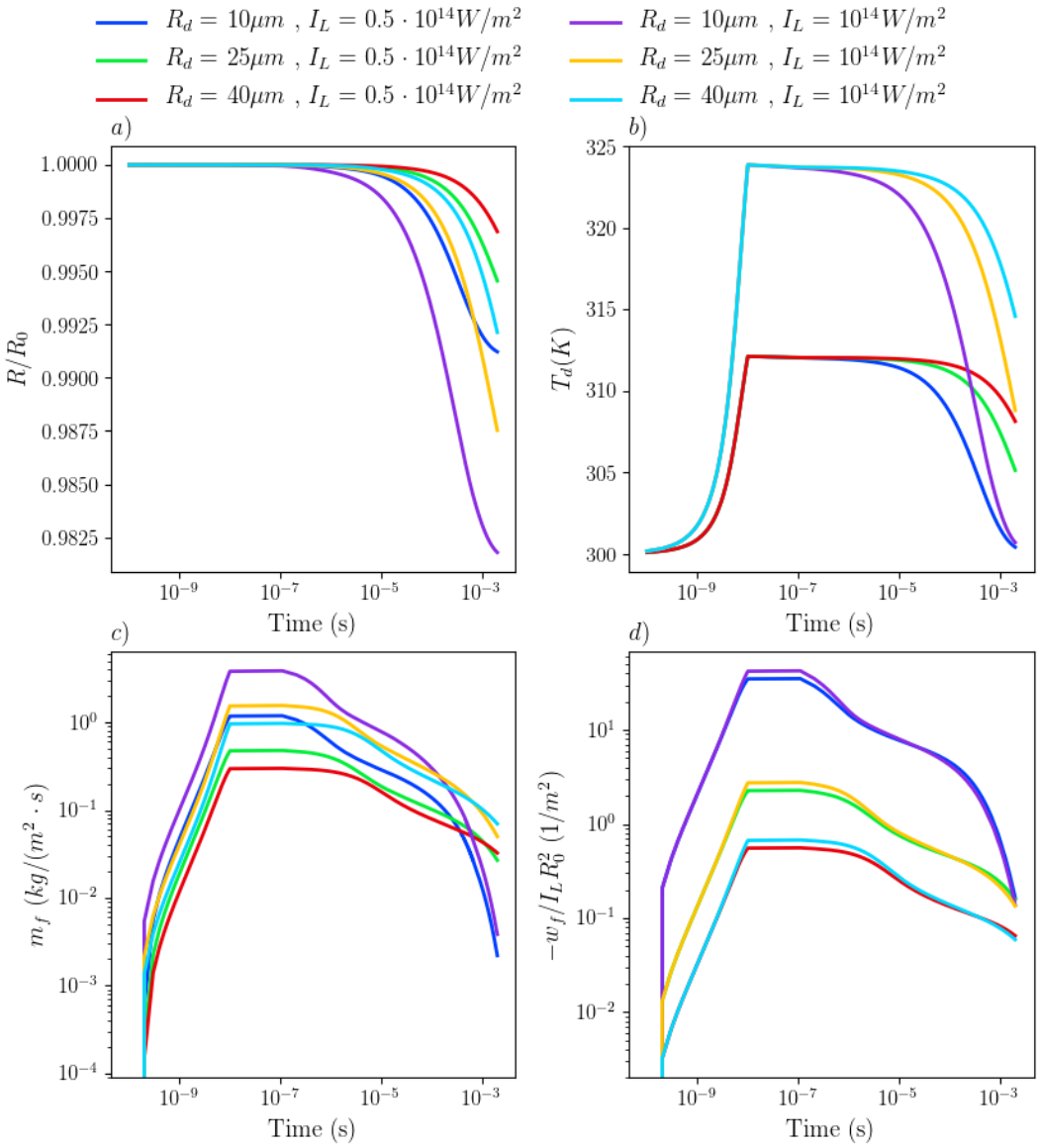


FIG. 12. Temporal evolution of ethanol droplet parameters; a) normalized radius, b) droplet temperature, c) evaporation mass flux, and d) conduction and convective heat flux normalized by $I_{L0}R_D^2$ for cases from Table I.

width half maximum, fwhm = 15 ns. The analytical result is slightly different from the simulation data due to the fact that the simulation results were for Gaussian pulses in time. Thus, if different pulse widths and peak intensities are chosen in such a way that the integrated intensity is the same, $fwhm = 15\ ns$, $I_{L0} = 2 \cdot 10^{14}\ W/m^2$ (triangle symbol) and $fwhm = 10\ ns$, $I_{L0} = 3 \cdot 10^{14}\ W/m^2$ (circle symbol), then the boiling temperature of the droplet is reached after the time equal to the same percentage of the pulse width. For both the laser pulses represented by the symbols in Fig.10 this time is 70% of the pulse width. As the integrated energy of the laser pulse in time determines when the droplet would reach the boiling temperature the temporal shape and peak intensity of the laser control the heating of the droplet.

For laser intensities below the critical irradiance temporal dynamics of the heating and evaporation process is shown in Fig.12. The mass fraction of ethanol and the induced velocity from the evaporation process for a case of pulsed laser heating, $fwhm = 10\ ns$, $I_{L0} = 1.0 \cdot 10^{14}\ W/m^2$ , $R_{D0} = 25\ \mu m$ , is shown in Fig.11. The strong radially symmetric gradient of the ethanol mass fraction at the interface, Fig.11 and a rapid increase in the temperature during the heating phase, Fig.12,b, are observed. After the end of the laser pulse, conductive and convective cooling of the droplet, which are relatively slow processes, leads to small changes in the droplet temperature over time. Qualitatively similar trend in the evolution of the droplet surface temperature was shown for the water droplet heated with a pulsed laser radiation[16]. It has been found, that

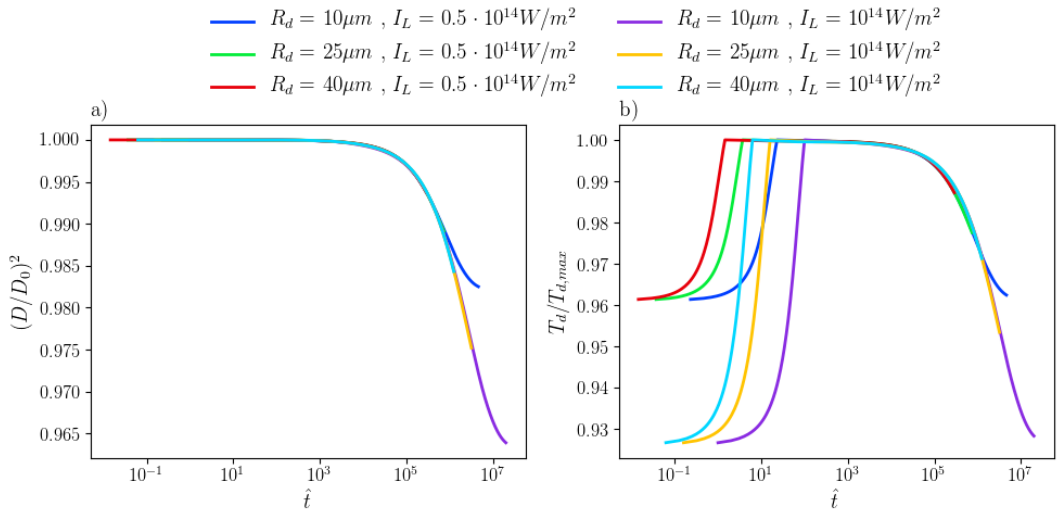


FIG. 13. Temporal evolution of ethanol droplet parameters for cases shown in table I; a) normalized surface area, b) droplet temperature normalized by maximum temperature. The normalized time $\hat{t} = t(I_{L0}/10^{14})^{2.11}/R_{D0}^2$

the maximum temperature of droplets heated by a short laser pulse does not depend on the droplet size and depends only on the peak intensity of laser radiation. This was not the case for continuous laser heating when the maximum temperature was reached later in time. Figure 12,d shows the conductive and convective heat flux from the droplet which is normalized by $I_{L0}R_D^2$. The normalized heat flux profiles for droplets of the same size followed a single profile for different intensities. It should be noted that without the normalization, the heat flux and mass flux, Fig.12,c trends were similar. This correlation between heat and mass transfer is often employed in semi-empirical models for droplet heating and evaporation. As seen from Fig.12,c the mass flux during the heating phase is higher for smaller droplets and for higher intensities in contrast to the smaller mass flux for smaller droplets only at the end of the cooling phase, $t \approx 1\ ms$. As a result, larger droplets cool slowly compared to smaller droplets after being heated to the same temperature, Fig.12,b. It is confirmed by the results shown in Fig.12, where temporal dynamics of the normalized radius for different size droplets is presented. The smallest droplets, $R_d = 10\ \mu m$, have lost all the energy gained from the laser pulse very quickly, and as a result, a decay of the normalized radius is practically flat at $t \approx 1\ ms$. The droplet being heated by a laser pulse of the higher maximum intensity , eg. $R_d = 25\ \mu m, I_{L0} = 10^{14}\ W/m^2$ is shrinking with the same rate approximately as the smaller droplet heated by a laser pulse of the smaller intensity, e.g. $R_d = 10\ \mu m, I_{L0} = 0.5 \cdot 10^{14}\ W/m^2$. From Fig.12 it is clear how the initial heating of the droplet proceeds, $t < 10^{-7}\ s$. But dynamics of heating and evaporation and their dependence on the droplet size and intensity of laser radiation are not clear for $t > 10^{-7}\ s$. However, the normalization of time as $\hat{t} = t(I_{L0}/10^{14})^{2.11}/R_{D0}^2$ gives results which are easier to interpret for later times as shown in Fig. 13. The results show that dynamics of the droplet shrinkage in terms of the surface area and cooling in terms of the normalized temperature with the proper time normalization follow the same dynamics for droplets of different sizes and peak laser intensities with the same pulse width. But when the temperature of the droplet is cooled to the ambient $\approx 300\ K$ the trend lines are separate as the droplet is close to equilibrium with the surrounding and does not evolve further in time.

The results for single pulsed heating of the droplet have distinct processes of initial heating and subsequent cooling and evaporation. In repeatedly pulsed operation, a single pulse laser operates similarly for heating and cooling of the droplets, but it provides more control with the ability to change the repetition rates. Now we consider pulsed laser heating when the laser wavelength, intensity and repetition rate are 1064 $nm$, $0.5 \times 10^{14}\ W/m^2$ and 100 KHz respectively. Five subsequent laser pulses of 10 ns pulse-width with a time delay of 10 $\mu s$ were employed for heating. It is seen that after each laser pulse the local linear evaporation regime, also called $D^2$ regime, is formed. But compared to the evaporation process from ambient surrounding heating, the slope of the square of the normalized droplet radius changes with time. Thus, instead of a constant evaporation rate we observed a gradually increasing evaporation rate. The faster cooling rate of smaller droplets causes higher temperature decrease compared to larger droplets in the cooling phase. This effect being accumulated during subsequent laser pulses causes transition to boiling regime for larger droplets while the smaller droplets are maintained well below the boiling temperature. This is clearly seen in Fig.14, b, where after the fifth laser pulse, droplets of $R_d = 25, 40\ \mu m$ undergo transition to the boiling mode but the smallest droplet with $R_d = 10\ \mu m$ does not. Thus, by changing the laser repetition rate it is possible to achieve a selective transition to the boiling regime for droplets of different sizes.

In summary, we show that heating and evaporation dynamics can be controlled by the laser operating parameters, such as

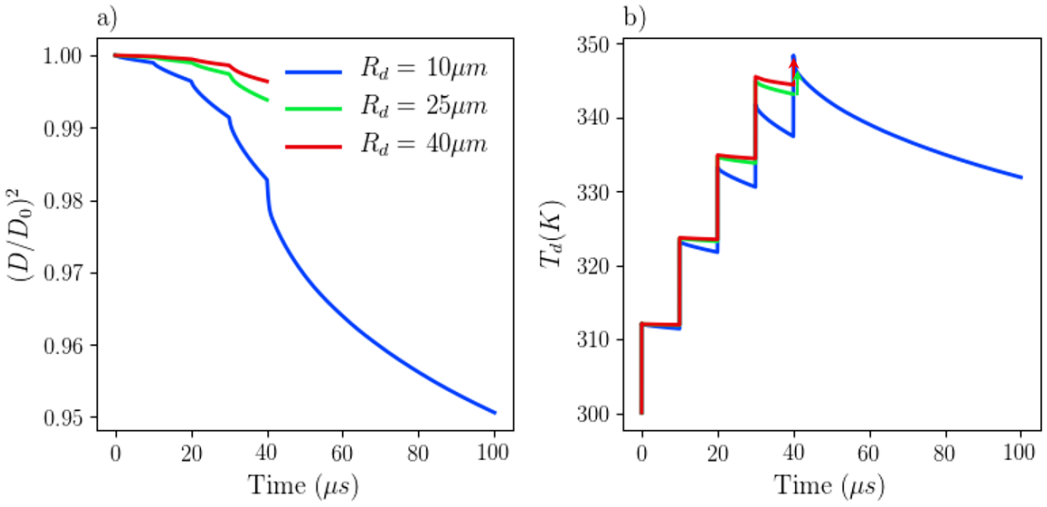


FIG. 14. Temporal evolution of a) normalized surface area and b) droplet temperature for pulsed laser heating of ethanol droplets $R_0 = 10\ \mu m, 25\ \mu m,\ 40\mu m$ with laser of $\lambda = 1064\ nm$, $I_0 = 0.5 \times 10^{14}\ W/m^2$, 100 KHz repetition rate.

a laser pulse width and a peak intensity. The temporal dependence of the cooling and shrinkage of the droplet can be made independent of droplet size using proper normalization of the time axis with the peak intensity of the laser. Further control over the droplet heating and evaporation dynamics, e.g, selective transition to boiling regime, can be achieved by the use of repeated laser pulses at a specified frequency.

### 3. *Semi-empirical relations*

To study laser heating and evaporation of the ensemble of droplets a more simplified model is attractive in terms of computational resources and robustness. Following the works in literature[16,18] we used a quasi-steady assumption and considered continuous laser heating to obtain the mass and heat flux at the droplet interface, which could be used in multi-dimensional calculations. Equation 2 can be solved using the expressions for the energy flux $\hat{w}_f = w_f/I_{L0}R_0^2$ and for the mass flux $m_f$ as follows

$$m_f = \frac{1}{R_D}\rho_g D_v ln\left(\frac{1-Y_{v,\infty}}{1-Y_{v,0}}\right)$$

$$\hat{w}_f = \frac{-C_{p,g}(T_D - T_{g,\infty})}{I_{L0}R_0^2} \cdot \frac{m_f}{exp(-(m_f R_D C_{p,g})/K_g) - 1} - \frac{m_f^3}{2I_{L0}R_0^2\rho_v^2}$$

Figure 15 shows the comparison between the results from the two-dimensional model and the simulation results with these semi-empirical expressions for fluxes. It is seen that the semi-empirical model predicts a higher peak temperature and shallower droplet shrinkage rate compared to the detailed model. But it captures the same temporal dynamics as observed in the detailed model. So the formulated expressions could be used as alternatives in studies related to an ensemble of droplets.

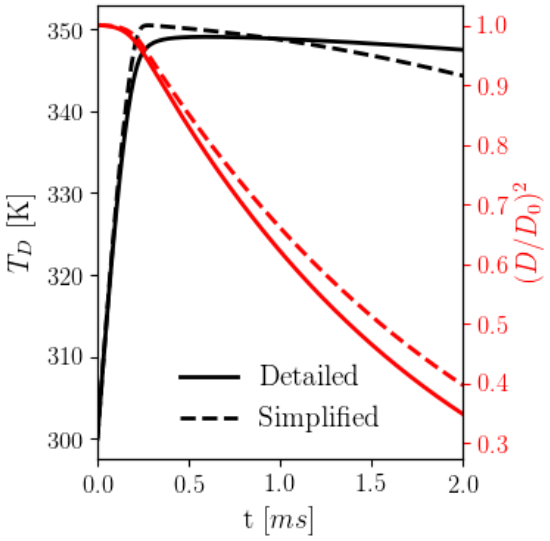


FIG. 15. Temporal evolution of the droplet temperature, left axis, and the normalized surface area, right axis for the detailed model(solid lines), and semi-empirical model (dashed lines). Results are shown for $R_D = 20\ \mu m$, $I_{L0} = 10^{10}\ W/m^2$ for the continuous laser heating case.

### 4. *Laser bleaching effect*

The absorption of laser radiation by liquid droplets suspended in gas makes it possible to use lasers for bleaching/clearing of the droplets along the laser propagation path.

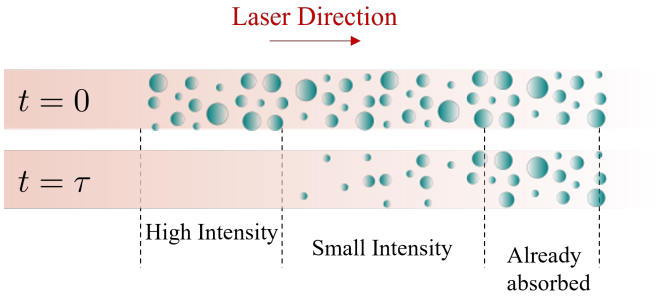


FIG. 16. Schematic showing the laser bleaching effect.

The desired path can be cleared of droplets to improve long range communication, remote sensing applications, etc. Based on the simulation results from previous sections we provide a qualitative description of the laser bleaching process. Consider a laser pulse propagating in air with some distribution of liquid droplets, Fig. 16. Liquid droplets exceeding the boiling temperature evaporate significantly faster[26] than droplets in diffusive mode of evaporation. Thus, we can identify three different regions along the laser path. The region close to the laser source is not attenuated and has a high intensity. In this region, droplets of all sizes ( $\approx$ microns ) evaporate very fast due to the transition to the boiling regime. The next region has smaller intensity due to the prior partial absorption of the laser radiation. In this region we have fast evaporation of larger droplets as they undergo transition to the boiling regime and a gradual decrease in size of remaining smaller droplets. With successive attenuation and diffraction spread at longer distances the effect of the laser radiation is not seen and droplets remain undisturbed. Thus, the gradual evaporation of droplets in time produces the bleaching effect.

## IV. CONCLUSIONS

A mathematical model for heating and evaporation of the isolated fuel droplet by continuous and pulsed laser irradiation has been developed. We extended the capabilities of OpenFOAMv6 by the addition of laser absorption, evaporation, thermophysical models, and custom boundary conditions. The developed solver accurately captured the dynamics of laser heating and evaporation of the ethanol droplet in the diffusion-dominated heating regime. For continuous laser heating, the ethanol droplet evaporated significantly faster compared to the water droplet and the peak temperature was higher for larger droplets. For continuous heating, a size of $R_{cr}$ exists for the specified laser parameters such that droplets of size, $R > R_{cr}$ undergo a transition to the boiling regime and rapid extinction while the droplets with $R < R_{cr}$ still maintain a slow decay of their size. For a single pulse laser heating with the peak irradiance close to the transition to the boiling regime, temporal dynamics of the droplet temperature followed the same dependence regardless of the droplet size. Appropriate normalization of time with the peak laser intensity unifies the dynamics of the droplet shrinkage and cooling for different droplet sizes and laser intensities. During the repetitive pulsed laser heating operation a selective transition to the boiling regime for larger droplets was observed. It should be noted that the inclusion of the evaporation process, conductive-convective cooling compared with the cases when all the absorbed energy goes to droplet heating significantly decrease the maximum droplet temperature and those effects cannot be neglected. Based on the simulated results, we have provided a quantitative explanation of the laser bleaching effect due to the absorption of laser radiation by the ensemble of droplets. The developed model and results, although mainly related to isolated ethanol droplets, are applicable to the ensemble of isolated droplets and to various liquids and should be beneficial for novel applications in laser propagation and remote sensing. Also, an increase of the laser intensity will lead to the ionization and laser plasma formation in the vapor layer, which will change the heat and mass transfer dynamics. This will provide an additional tool to control heating and evaporation processes using the laser pulse and needs further investigation.

## ACKNOWLEDGMENTS

This work is partially supported by the Princeton Collaborative Research Facility (PCRF), supported by the U.S. Department of Energy (DOE) under Contract No.DE-AC02-09CH11466. S.P. and A.T. also acknowledge support from the U.S. DOE Office of Science Award No.M2103358/28-520010. Part of this research was conducted using the advanced computing resources of the TERRA clusters provided by Texas A&M High Performance Research Computing.

## DATA AVAILABILITY STATEMENT

The data that support the findings of this study are available from the corresponding author upon reasonable request.

## Appendix: Thermo-physical and Optical Properties

### 1. Ethanol Liquid

Latent Heat of vaporization, $[J/kg]$:
$L = 1.0947 \cdot 10^6 \exp\left(0.4475\,(T/513.9)\right)(1 - T/513.9)^{0.4989}$

Specific heat capacity in $[kJ/(kg \cdot K)]$, where $\tau = T/1000$.
$Cp,l = 1.04721599 + 15.6271404\ \tau - 107.941020\ \tau^2 + 310.825090\ \tau^3 - 241.911840\ \tau^4$

Density, $[kg/m^3]$.
$\rho_l = 276 \cdot (0.27688)^{-(1-T/516.25)^{0.23670}}$

### 2. Ethanol vapor

Diffusivity in air, $[m^2/s]$.
$D_{v,a} = \left(-0.10107 + 5.6275 \cdot 10^{-4} T + 5.8314 \cdot 10^{-7} T^2\right) \cdot 10^{-4}$

Thermal conductivity, $[W/(m \cdot K)]$.
$K_v = -1.3405 \cdot 10^{-2} + 7.0239 \cdot 10^{-5} T + 9.0124 \cdot 10^{-8} T^2 - 3.6957 \cdot 10^{-11} T^3$

Dynamic viscosity , $[Pa \cdot s]$.
$\mu_v = (1.8086 + 3.0504 \cdot 10^{-1} T - 3.9837 \cdot 10^{-5} T^2 - 2.5788 \cdot 10^{-9} T^3) \cdot 10^{-7}$

### 3. Optical Properties

Ethanol refractive index, at $\lambda = 1064\ nm$
$n = 1.3547 - i9.6524 \cdot 10^{-7}$

Water refractive index, at $\lambda = 1064\ nm$
$n = 1.326 - i1.15 \cdot 10^{-6}$

Water refractive index, at $\lambda = 10.6\ \mu m$
$n = 1.179 - i0.0852$


[1] J. Reutzsch, C. Kieffer-Roth, and B. Weigand, "A consistent method for direct numerical simulation of droplet evaporation," Journal of Computational Physics **413**, 109455 (2020).

[2] S. S. Sazhin, "Modelling of fuel droplet heating and evaporation: Recent results and unsolved problems," Fuel **196**, 69–101 (2017).

[3] F. A. Williams, *Combustion theory* (CRC Press, 2018).

[4] S. Sazhin, W. Abdelghaffar, P. Krutitskii, E. Sazhina, and M. Heikal, "New approaches to numerical modelling of droplet transient heating and evaporation," International journal of heat and mass transfer **48**, 4215–4228 (2005).

[5] S. Tonini and G. Cossali, "An exact solution of the mass transport equations for spheroidal evaporating drops," International Journal of Heat and Mass Transfer **60**, 236–240 (2013).

[6] B. Abramzon and W. Sirignano, "Droplet vaporization model for spray combustion calculations," International journal of heat and mass transfer **32**, 1605–1618 (1989).

[7] P. Bruggeman, M. J. Kushner, B. R. Locke, J. G. Gardeniers, W. Graham, D. B. Graves, R. Hofman-Caris, D. Maric, J. P. Reid, E. Ceriani, *et al.*, "Plasma–liquid interactions: a review and roadmap," Plasma sources science and technology **25**, 053002 (2016).

[8] Y. Asakawa, "Promotion and retardation of heat transfer by electric fields," Nature **261**, 220–221 (1976).

[9] J. M. Bergthorson and M. J. Thomson, "A review of the combustion and emissions properties of advanced transportation biofuels and their impact on existing and future engines," Renewable and sustainable energy reviews **42**, 1393–1417 (2015).

[10] M. Al Qubeissi, N. Al-Esawi, S. S. Sazhin, and M. Ghaleeh, "Ethanol/gasoline droplet heating and evaporation: Effects of fuel blends and ambient conditions," Energy & fuels **32**, 6498–6506 (2018).

[11] A. P. Pinheiro, J. M. Vedovoto, A. da Silveira Neto, and B. G. van Wachem, "Ethanol droplet evaporation: effects of ambient temperature, pressure and fuel vapor concentration," International Journal of Heat and Mass Transfer **143**, 118472 (2019).

[12] L. Dombrovsky and S. Sazhin, "Absorption of thermal radiation in a semi-transparent spherical droplet: a simplified model," International journal of heat and fluid flow **24**, 919–927 (2003).

[13] L. Dombrovsky, S. S. Sazhin, and M. R. Heikal, "Computational model of spectral radiation characteristics of diesel fuel droplets," Heat Transfer Research **35** (2004).

[14] W. Hergert and T. Wriedt, *The Mie theory: basics and applications*, Vol. 169 (Springer, 2012).

[15] B.-S. Park and R. L. Armstrong, "Laser droplet heating: fast and slow heating regimes," Applied optics **28**, 3671–3680 (1989).

[16] S. Davies and J. R. Brock, "Laser evaporation of droplets," Applied optics **26**, 786–793 (1987).

[17] B. Abramzon and S. Sazhin, "Droplet vaporization model in the presence of thermal radiation," International Journal of Heat and Mass Transfer **48**, 1868–1873 (2005).

[18] A. Zardecki and R. L. Armstrong, "Energy balance in laser-irradiated vaporizing droplets," Applied optics **27**, 3690–3695 (1988).

[19] D. E. Rosner, *Transport processes in chemically reacting flow systems* (Courier Corporation, 2012).

[20] T. Khasanshin and A. Aleksandrov, "Thermodynamic properties of ethanol at atmospheric pressure," Journal of engineering physics **47**, 1046–1052 (1984).

[21] C. L. Yaws, *Thermophysical properties of chemicals and hydrocarbons* (William Andrew, 2008).

[22] C. L. Yaws, *Transport properties of chemicals and hydrocarbons* (William Andrew, 2014).

[23] S. Kedenburg, M. Vieweg, T. Gissibl, and H. Giessen, "Linear refractive index and absorption measurements of nonlinear optical liquids in the visible and near-infrared spectral region," Optical Materials Express **2**, 1588–1611 (2012).

[24] H. Jasak, "Openfoam: open source cfd in research and industry," International Journal of Naval Architecture and Ocean Engineering **1**, 89–94 (2009).

[25] S. B. Saharin, B. Lefort, C. Morin, C. Chauveau, L. Le Moyne, and R. Kafafy, "Vaporization characteristics of ethanol and 1-propanol droplets at high temperatures," Atomization and Sprays **22** (2012).

[26] A. N. Kucherov, "Clearing of a polydisperse water aerosol by a laser pulse in the diffusive—convective regime," Quantum Electronics **36**, 363 (2006).